Chapter 6

Numerical models of deformation and fluid flow across basement-cover interfaces during extension-related mineralisation

Acknowledgement of Contributions

This chapter is intended for future publication in the SEG 100th Anniversary Volume (late 2004)

Contributions made to this chapter involved:

J. G. McLellan – Geomechanical Modelling

N.H.S. Oliver – Conceptual idea for the article, research and background text, and normal supervisory conditions.

J. G. McLellan – 10% (p. 249-256), 90% (p. 256-283)

N.H.S. Oliver – 90% (p. 249-256), 10% (p. 256-283)

This work will be compiled with additional work by

J. S. Cleverley, L. Feltrin and B. E. Hobbs

and submission of this article is proposed as:

Oliver, N.H.S., McLellan, J.G., Cleverley, J.S., Feltrin, L., Hobbs, B.E., 2004. Numerical models of deformation, fluid flow and mass transfer across basement cover interfaces during extension-related mineralisation. SEG 100th Anniversary Volume, xxxx.

Abstract

Extension related deformation and its effects on fluid flow are tested here by numerical models of basement-cover interfaces, faults and variations in strain rates. Finite difference modelling of coupled deformation and fluid flow with FLAC (Fast Lagrangian Analysis of Continua) was used to explore the mechanical responses to extensional deformation as a process driving fluid migration into and outward of basement material underlying sedimentary basins. Simple models of permeable cover and low permeable basement display a rapid decrease in pore pressure in both cover, and in particular basement material, at high strain rates. When strain rates are reduced a more gradual decrease in pore pressure is seen, with the system approaching a state of hydrostatic equilibrium. Contrasts in permeability, between the basement and sedimentary cover, prevent any significant exchange of fluid between these units. The addition of permeable structures, such as faults or shear zones, across the basement-cover interface facilitates fluid migration between these two units. When a hydrostatic pore pressure gradient is applied to the whole model, downward migration of fluid flow, as a result of extension, is apparent. A lithostatic gradient in the basement provides an overpressure which aids in upward migration of fluid until the system reaches a critical point (nearing hydrostatic pore pressure in the basement) then a reversal of flow direction is apparent. It is clear that slower strain rates aid in maintaining pressure gradients, allowing time for the system to equilibrate, however rapid decreases in pressure as a result of dilation and failure may provide insights into episodic and rapid deformation processes found in some geological systems. In particular, if fluid flow rates are insufficient to keep up with high strain rates

(particularly in low permeability basement); down flow is a consequence of extension.

6.1 Introduction

Active extension plays a role in the hydrology of many ore forming systems both at the surface and in the subsurface (e.g. Russell, 1986; Beaudoin ***et al***., 1992; Morrison, 1994; Oliver, ***et al***., 1994). Although this general relationship has been understood for many years, uncertainties remain, particularly in the following areas:

- What was the contribution of the basement to the mass and fluid budget of the system?
- If basement was involved, how was mass extracted from the basement to make its way into the cover sequences hosting mineralisation?
- Is convection important and are basement rocks involved in the circulation?
- What roles do hinterland topography, erosion, extension and contraction have on the potential for fluids to leach, transport and precipitate metals in ore concentrations?

The aim of this chapter is to explore a few of these issues using published examples of different types of extension-related mineralisation in combination with finite element modelling of the response of fluid flow to deformation, and variable permeability structures. In parallel with this research on mechanical behaviour, modelling of convection in porous media is being used to compare with the deformation-related effects demonstrated here (Oliver, ***et al***., ms. see p. 145).

6.2 Geological Context

In Neogene/Paleogene ***core complexes*** of western North America, widespread potassic alteration occurs in conjunction with precious and base metal mineralisation in the hangingwall of detachment faults. Several authors have proposed that deep-seated, reduced fluids mixed with shallow, oxidised fluids near detachments, culminating in mineralisation. For example, in the Kokanee Range in British Columbia, Beaudoin ***et al.*** (1992) inferred, using a combination of Pb and stable isotopes, that fluid mixing was a primary cause of mineralisation. Some of the Pb and C was thought to be derived from the mantle via a transcrustal fault zone, and some from convecting upper crustal fluids. Nesbitt, ***et al***. (1995) also proposed convection to explain the apparent intensity of alteration and diversity of isotope ratios and admixture of metamorphic CO2 with near-surface fluids. They also pointed out the low permeabilities of basement rocks as a likely limit to the depth of convection. Spencer & Welty (1986) focussed on elevated geotherms caused by the hot lower plate, and mixing at normal fault ramps of ascending reduced fluids and descending oxidised fluids. In this model, protracted and focussed metal accumulation at redox interfaces was achieved by progressive fault displacements permitting mixing reactions to occur in a similar location over time. Other models for core complexes have proposed that near-surface fluids penetrated into lower, ductile plates during active extension (e.g. Wickham & Taylor, 1985; Morrison, 1994).

Stratabound Pb-Zn deposits are mostly thought to form in the latter stages of rifting cycles by interaction of near-surface brines with deeper rocks, scouring

base metals from the basement and/or the deeper sedimentary pile, followed by upflow and mixing of such brines with ocean floor or near-surface fluids and rocks causing sulphide precipitation (Large, 1980). Bjørlykke ***et al***., (1991) notes an important role for basement rocks in such settings, pointing out the widely variable Pb-isotope signatures for such deposits worldwide. Similar observations have been made for ***Irish Base Metal*** deposits, with (Everett, ***et al.,*** 2003) proposing that basement must have been scoured to provide the characteristic Pb-isotope signature of the ores. There is some uncertainty about the timing of mineralisation, with models ranging from syn-extensional (Russell, 1986) through to transitional and very early contractional (Johnston, 1999). Johnston (1999) noted the confluence of many of the major deposits with parts of the cover sequence lying above reactivated basement faults and intersections, also proposing that basement may have provided much of the metals by transtensional reactivation of basement structures. Russell (1986) proposed that extension facilitated the penetration of convection cells into fault zones cutting the basement to the Irish base metal deposits, and proposed mixing of the deeply convected modified seawaters with shallow sulfurous brines to produce the deposits. Many other deposit models have appealed to mixing of near-surface and deeper seated fluid, metal and sulphur during extension, including post-collisional ***Alpine-style base metal, fluorite and barite vein deposits*** (e.g. Johnson, 1996; de Boorder ***et al.***, 1998), ***back-arc volcanic-hosted massive sulphide deposits*** distal to retreating or rupturing subducted slabs (Crawford ***et al.***, 1992; Zengqian & Liquan, 2003) and ***unconformity-related uranium deposits*** (Hein, 2002). Most models for ***Archean and early Proterozoic lode-gold deposits*** appeal to late-orogenic contraction or strike-slip

movement to focus gold-bearing fluids; however Chauvet ***et al.*** (2001) proposed that post-orogenic extension was responsible for gold mines in parts of the Iron Quadrangle in Brazil. Although the diverse family of ***iron-oxide-Cu-Au deposits*** have apparently equally diverse tectonic settings (Williams ***et al.***, 2005), Oyarzun ***et al.*** (1999) speculated that Candelaria in Chile may have formed by interaction between lower plate granite-derived fluids and upper plate brines during syn-intrusive extension. Traditional models for supergene enrichment in stable continental environments to explain ***giant iron ore deposits*** of microplaty hematite in Western Australia and the Iron Quadrangle in Brazil have been challenged in recent years by models appealing to deep penetration of surface fluids during late- or post-orogenic extension, mixing with or overprinting reduced, basement-derived fluids (Powell ***et al.***, 1999; Taylor ***et al.***, 2001; McLellan ***et al.***, 2004).

The general mechanics of extensional faulting, orogenic collapse, core complexes and basin formation are fairly well understood at a range of scales (e.g. Wernicke, 1981; England & Houseman, 1988; Lister & Davis, 1989; Malavieille & Taboada, 1991; de Boorder ***et al.***, 1998), and have also been the subject of a range of analogue and numerical models (e.g. McClay & Ellis, 1987; Buck & Lavier, 2003). Hydrodynamic models for extension are considerably fewer. Some classic hydrodynamic models for topographic or compaction-driven flow have predicted that flow should largely be restricted to the relatively permeable, mostly saturated sediment package defining the main part of a particular basin (e.g. Garven & Freeze, 1984b). The apparent conflict between our understanding of basinal permeability structure and the

contribution of “impermeable” basement to the isotopic and metallogenic character of extension-related ore deposits has lead to various solutions proposing that basinal fluid flow can be fed by a) periodic upward pulses of fluid from basement penetrating faults, or b) by downward penetration of dense brines into the basement, then up again, potentially by convection (Russell, 1986; Reynolds & Lister, 1987; Dixon ***et al.***, 1991; Schmitt ***et al.***, 1991; Garven ***et al.***, 2001).

Deep drilling of Kontinentales Tiefbohrprogramm der Bundesrepublik Deutschland (KTB) in Germany and the Kola Superdeep Borehole in Russia revealed hydrostatically pressured fluids on fracture networks deeper than 8 km in “inactive” continental crust (e.g. Möller ***et al.***, 1997), contrasting with oilfield observations of overpressure in compacting sedimentary basins as shallow as 3 km (Moore ***et al.***, 1995). Subhydrostatic pore pressures and downward migration of fluids have been revealed in the German KTB due to H_20 consuming reactions e.g. zeolitization of feldspar (Stober & Bucher, 2004). For extensional systems in which compacting or compacted sedimentary basins lie above basement rocks with fracture networks, there are no natural examples of the fluid pressure variations across this interface – the KTB and Kola deep holes penetrated only fractured cratonic basement whereas the oilfields drillholes did not penetrate into basement. Here, we will build on earlier work dealing with the nature of fluid flow across and around the basement/cover interface (e.g. Reynolds & Lister, 1987; Dixon ***et al.***, 1991; Oliver ***et al.***, 1994), and recent numerical modelling by McLellan ***et al.*** (2004), who have specifically considered the mechanical effects of fluid flow in the extending environment.

The aim is to better understand the ways in which basement and cover may interact hydrodynamically during extension, and how this interaction may lead to mineralisation in the cover.

6.3 Numerical Modelling

We use here the finite difference code FLAC (Fast Lagrangian Analysis of Continua, (Cundall, 1988) which is best suited for modelling porous–media style fluid flow through deforming elasto-plastic rock masses. FLAC is a two-dimensional code that treats rock masses as though they are continua represented by average values of mechanical, fluid flow and heat transport properties in plane stress or plane strain conditions, and a three-dimensional version is also available. FLAC also treats faults as having continuous, rather than discontinuous properties (e.g. Ord 1991a; Ord & Oliver, 1997). Pre-ordained fault zones, for example, can be inserted as bands of high permeability grid blocks with fault- or shear-like input parameters. Localised fault zones or deformation bands may also appear during the course of model runs from within previously homogeneous materials. These zones have realistic appearances and properties of shear zones that have been verified against experimental data (Ord, 1991a; Ord, 1991b). The geological and numerical basis for the FLAC modelling is covered in detail by Ord & Oliver (1997) and in Chapter 2 here; FLAC has been utilised by us and others in several recent studies and syntheses of deformation-related fluid flow in mineralised rocks (Oliver ***et al.***, 1999; Oliver ***et al.***, 2001a; McLellan ***et al.***, 2004).

The fluid obeys Darcy's Law; permeability can be fixed for given rock types or allowed to change as a function of the deformation. The porosity has two components, the first being a FLAC–defined porosity which is strain–independent, the second being related directly to the volume change occurring during deformation. The volume change during deformation (and the linked porosity change) is conceptualised by the dilation angle, which is a measure of the propensity of a rock to dilate during deformation. The increase in pore volume during deformation arises from the sliding of irregular surfaces past each other, such as along grain boundaries and fractures surfaces (e.g. Brace, 1968; Ord, 1991a). Common rocks such as sandstones and marbles have experimental determined dilation angles on the order of +10 to +20°; some strong rocks (e.g. gabbro, skarn) may be greater; highly porous limestone and similar rocks may even have negative dilation angles.

Volume changes due to deformation of dilatant materials give rise to pore pressure changes, thence changes in the hydraulic head and fluid flow according to Darcy's Law. Changes in effective stress due to volume change can lead to elasto-plastic deformation, which in turn leads to changes in volume. Feedback between fluid flow and deformation thus continues. Simulations of compacting sedimentary basins in which deformation typically leads to expulsion of fluid by poro-elasticity, would require different constitutive properties for rocks and fluids than modelled here (e.g. Ge & Garven, 1992). Thus, here we are considering only behaviour of already compacted materials which show elasto-plastic behaviour and a tendency towards fluid being drawn into dilatant deformation zones.

6.4 Extension and Basin Formation

Fluid flow during basin formation may be regarded as essentially two-stage (e.g. Domenico & Schwartz, 1997): an early stage in which compaction in the basin core drives fluid outwards to its margins, and a later stage when compacted sediments are replenished by influx of meteoric water as the basin margins are exhumed. In the later stage, fluids may also be added to the deeper parts of the system by diagenetic and metamorphic reactions, and in this deeper realm both hydrocarbon maturation and metal leaching may occur. However, these classic models for basin formation do not consider the role of basement.

6.5 Conceptual Models

Several conceptual models were investigated that could provide an insight into how topography and permeable shear zones influence fluid flow during extensional deformation. These conceptual models firstly investigated the effect of topographic fluid driving forces (see Chapter 3 – Model 1). We then investigated simple block models that variable pore pressure starting conditions. A simple block model (Model 1) (Fig. 6.1a), 12 km wide by 8 km deep, included a basement-cover (granite-sediment) interface; a variant of this model was firstly initialised at hydrostatic pore pressures and then deformed. The basement was then initialised at lithostatic pore pressures (with the cover remaining at hydrostatic) to examine the effect of overpressure on fluid flow migration. Variations of these models were also run to inspect the consequences of different permeability contrasts across this interface. Models were then constructed to examine the behaviour across this interface with the

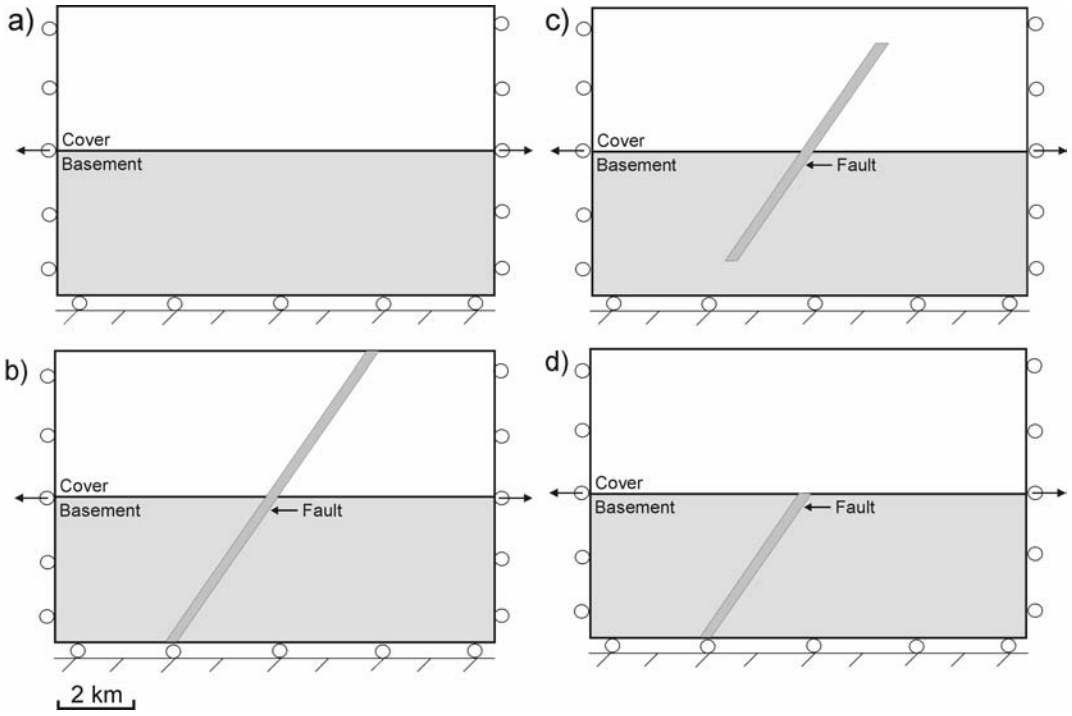

Figure 6.1. Four basic geometric considerations as conceptual models (12 km x 8 km), **a**) basic block model with basement-cover interface, **b**) addition of a permeable fault, **c**) short fault with no boundary contact, and **d**) basement only fault. All models are deformed in extension.

addition of a permeable shear zone (Model 2) (Fig. 6.1b), with variations on the pore pressure (similar to Model 1) and also to the extent of the shear zone into basement and sedimentary cover (Fig. 6.1c,d). Boundary conditions of the models were commensurate with extensional deformation. As a final analysis, the strain rates of deformation were investigated to examine what influence this had on pore pressure distributions and fluid flow. All material properties for these models are given in Table 6.1.

Table. 6.1. Material properties for FLAC coupled deformation and fluid flow models.

Model	Density	Bulk modulus	Shear modulus	Cohesion	Friction angle	Dilation angle	Permeability
	(kg/m^3)	(Pa)	(Pa)	(Pa)	(°)	(°)	(m^2)
Models 1 and 2							
Sediments (Cover)	2400	3.20e10	1.92e10	4.00e6	30	4	1.00e-13
Granite (Basement)	2650	4.95e10	2.97e10	4.00e6	30	4	2.00e-16
Fault	2400	2.81e10	1.69e9	3.00e3	30	4	1.00e-14

6.6 Results

6.6.1 Model 1a (Extension - Hydrostatic pore pressure)

The initial block model was initialised at hydrostatic pore pressures and run to equilibrium (Fig. 6.2a) before extensional deformation was applied. At early stages of deformation, fluid flow within the model was noted to be in a downward direction and closely associated with developing shear bands and dilation (Fig. 6.2b). Fluid flow was seen to decrease by around 2 orders of magnitude at the basement-cover interface (3.537e-7 ms^{-1} sediment cover, and 7.15e-9 ms^{-1} in the basement), primarily due to permeability contrasts. As extension progressed to around 6%, four distinct conjugate shear bands formed which focused fluids within them, particularly in the cover (Fig. 6.3a), however the basement showed no significant fluid flow due to the low permeability values assigned. As a result of deformation and dilation, or volume increase within the model, pore pressures decayed, particularly within the basement rocks. Fluid flow displays a predominant downward migration in the cover and into the top of the basement, and mainly focused towards areas of low pore pressure (Fig. 6.3b).

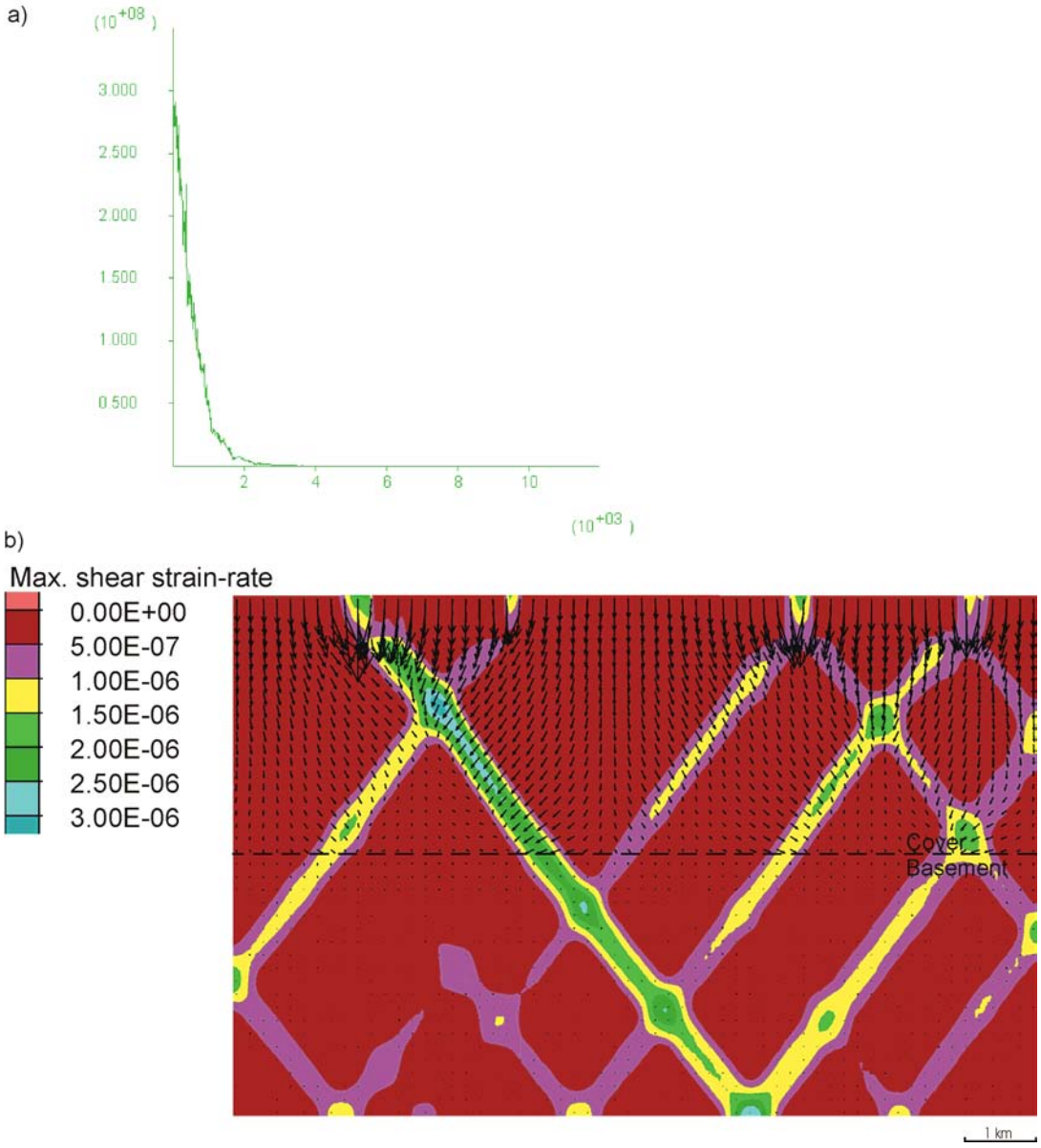

Figure 6.2. Model 1a, plots of **a**) unbalanced history prior to deformation, **b**) shear strain rate at 2% extension, displaying conjugate shear bands throughout the model. Fluid flow is downward and closely associated with areas of high shear strain. Flow velocities decrease in the basement relative to the cover, as a consequence of the lower permeability values.

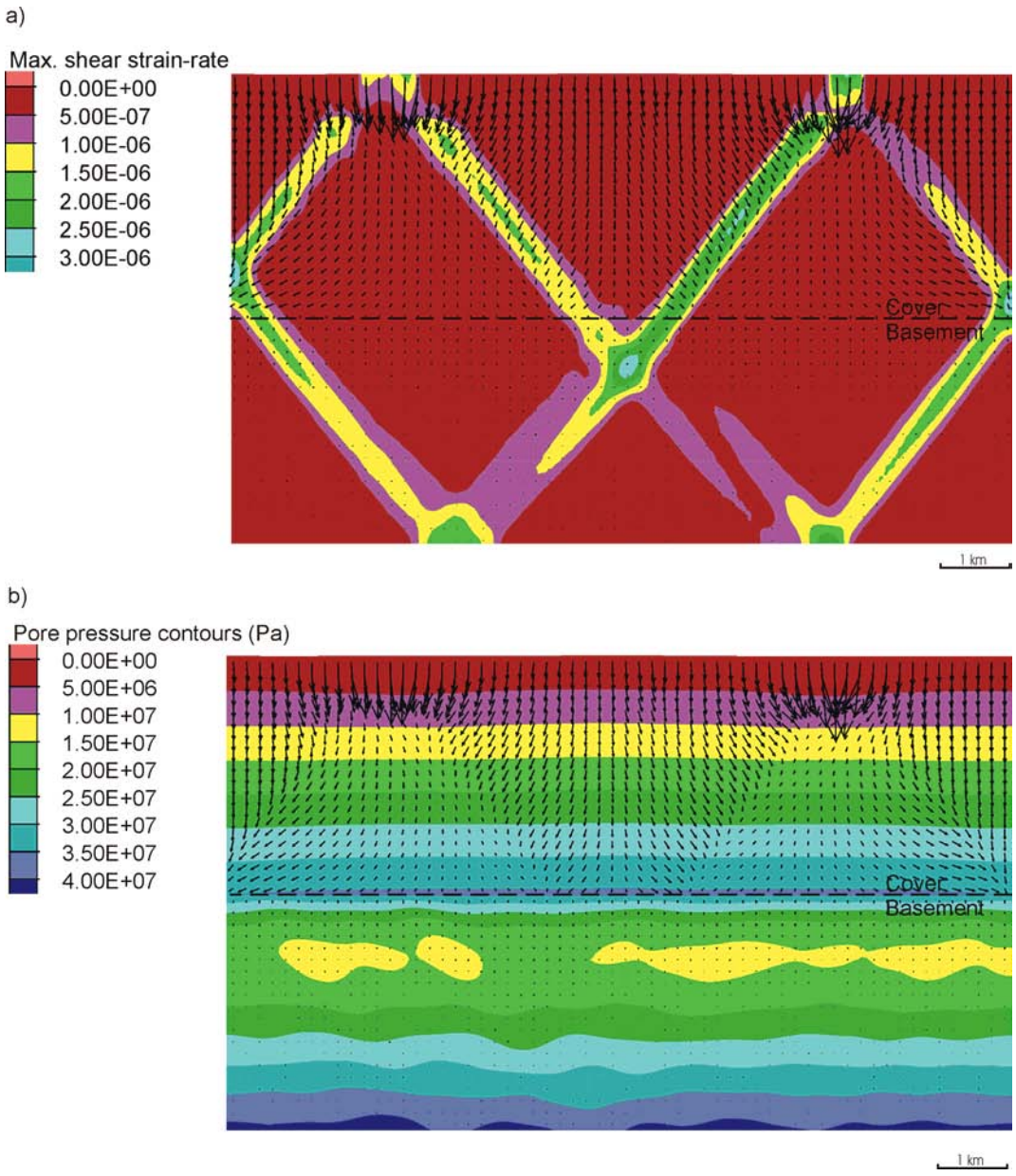

Figure 6.3. Model 1a at 6% extension, plots of **a**) shear strain rate, note as deformation progresses four major shears develop which focus fluid flow particularly in the ore permeable cover, **b**) pore pressure contours, indicating a broad band of pore pressure decay across the model, particularly below the basement-cover interface.

6.6.2 Model 1b (Extension - Lithostatic pore pressure in the basement)

This model has the same basic properties as the previous model; however pore pressure within the basement rocks was initialised at lithostatic values and a

higher ratio of fluid to mechanical steps were applied to the model (10 fluid steps to 1 mechanical step), in an attempt to maintain pore pressure. At early stages of deformation (2%) we can see that pore pressure has decayed in the basement but not in the cover (Fig. 6.4a). Fluid flow is primarily in an upward direction from both the basement and cover and driven by shear bands forming in the model, although downward flow is noted within the top half of the cover, driven by areas of failure and dilation (Fig. 6.4b).

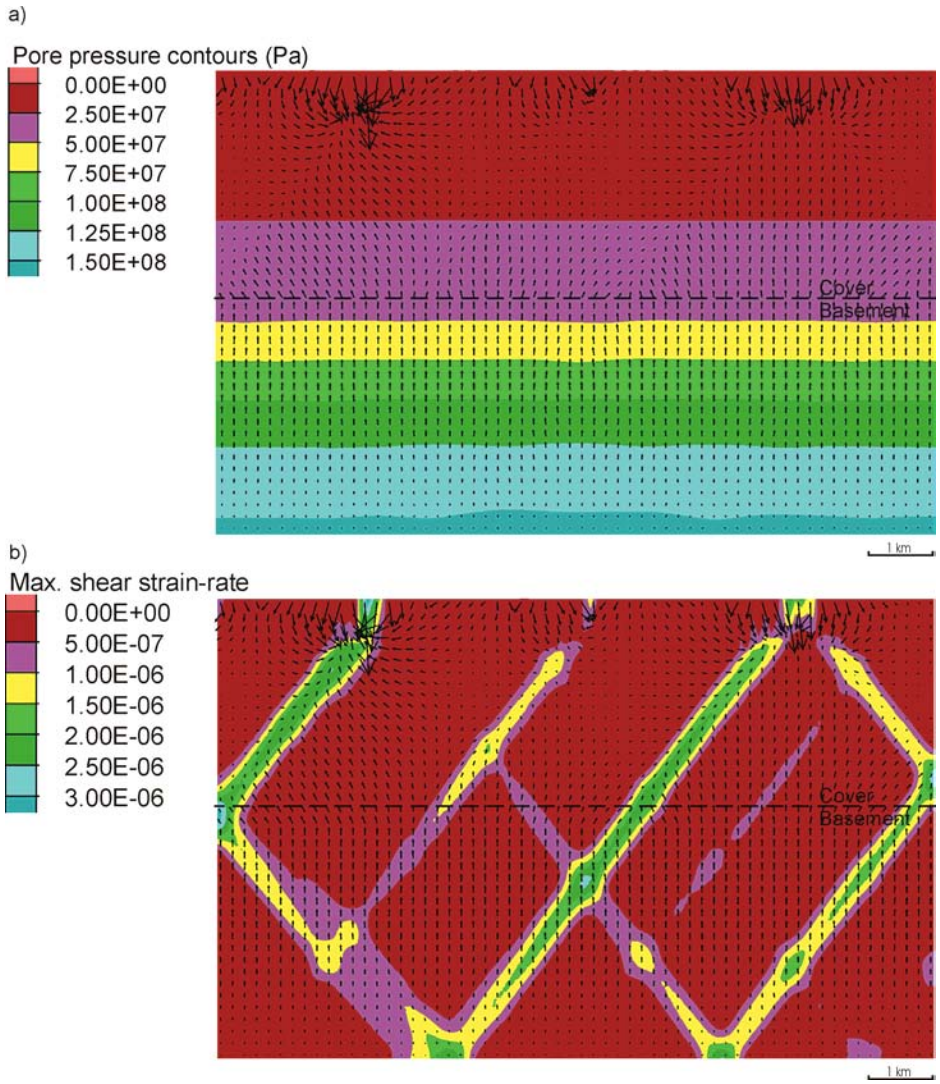

Figure 6.4. Model 1b at 2% extension, **a**) pore pressure contours indicating a relatively stable hydrostatic gradient in the cover, however, pore pressure has decayed from initial lithostatic pressure in the basement. Fluid flow direction is primarily upward in most of the model, however the top of the cover displays downward migrating fluids, **b**) shear strain rate, displaying a different distribution relative to Model 1a.

As extension progresses pore pressure within the model decays towards hydrostatic values (Fig. 6.5a) and fluid flow within the model displays a downward direction in the cover and upward in the basement (Fig. 6.5b), however little to no fluid enters the basement in this model.

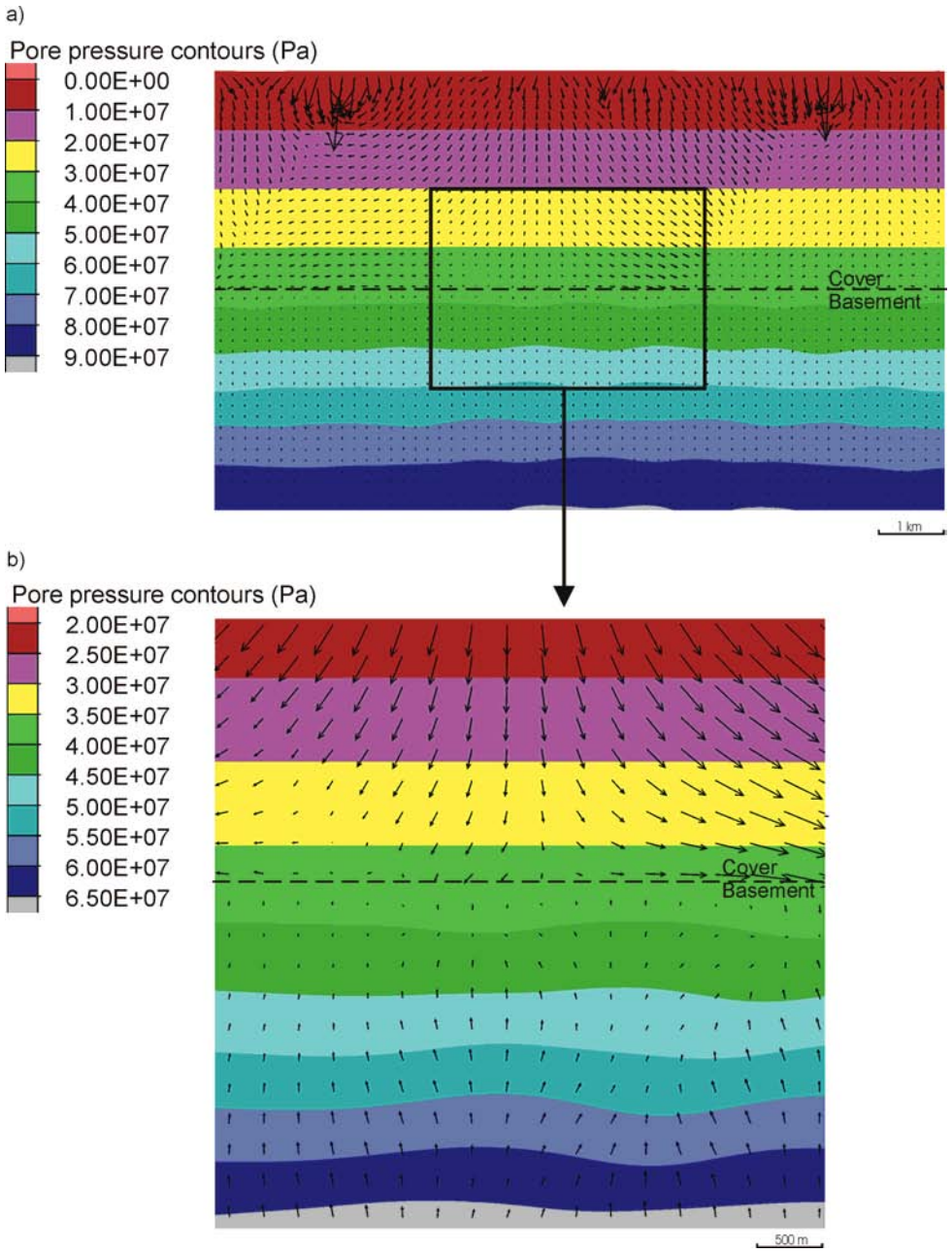

Figure 6.5. Model 1b at 6% extension, **a**) pore pressure contours indicating a relatively stable hydrostatic gradient in the cover, and pore pressure has decayed to slightly above hydrostatic in the basement. Fluid flow direction is primarily downward in the cover and upward in the basement, **b**) magnification at the interface displaying pore pressure contours and fluid flow vectors.

6.6.3 Model 2a (Extension - Hydrostatic pore pressure with fault)

When a fault is introduced to the model it provides a structure for localisation of strain, which becomes dilatant and focuses fluid flow (Fig. 6.6a). At 2% extension, a decrease in pore pressure is apparent, particularly in the granite beneath the cover-basement interface (Fig. 6.6b).

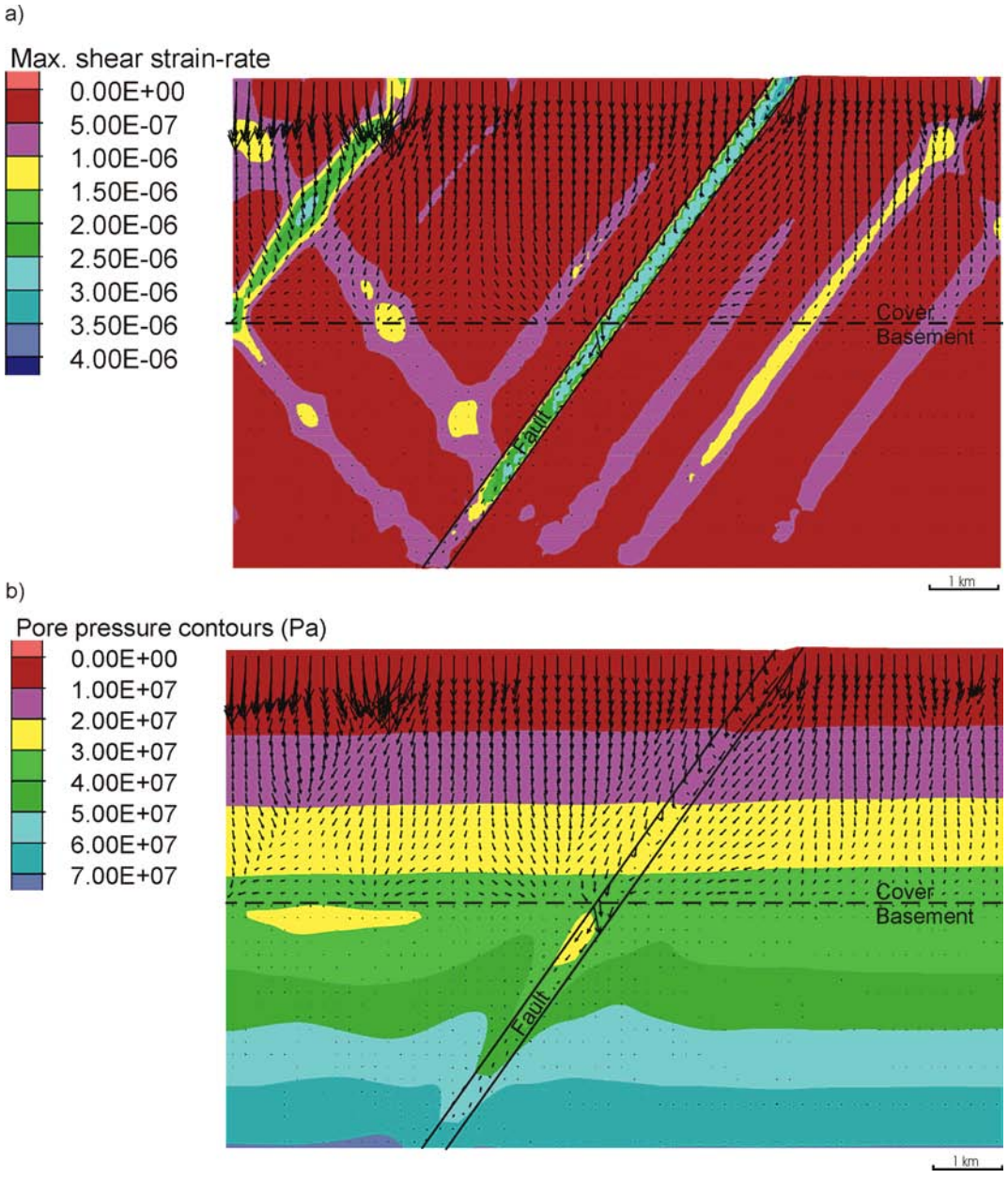

Figure 6.6. Model 2a at 2% extension, **a**) shear strain rate showing maximum values in the fault which coincides with maximum dilation and result in fluid flow focussing, **b**) pore pressure contours and fluid flow vectors, displaying an overall decrease in pore pressure. Subhydrostatic gradients are evident in the basement and fluid is focussed within the more permeable fault.

Fluid is primarily focussed towards dilatant areas and can be seen to be driven downwards from the cover by the influence of newly formed topography (Fig. 6.7), and also by deformation induced dilatancy.

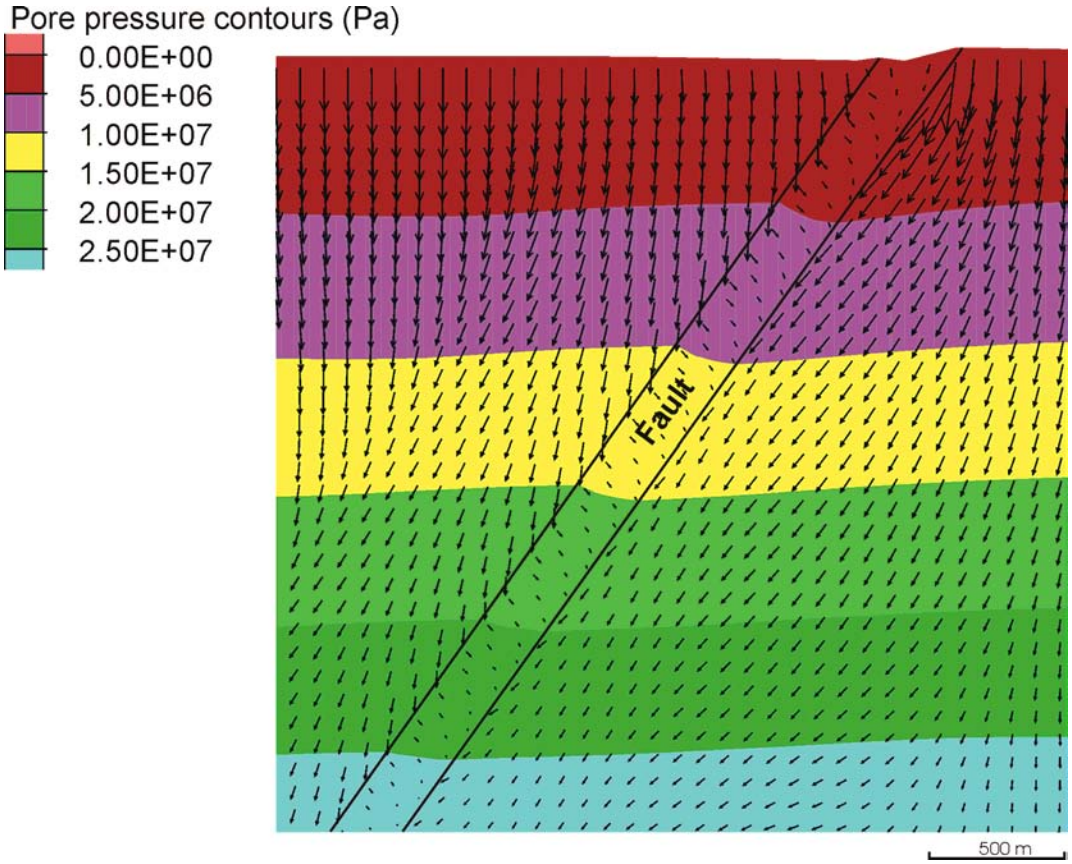

Figure 6.7. Model 2a at 2% extension, displaying pore pressure contours and displacement on the fault at the top of the model. Fluid is driven in a downward migration by topographic influence in combination with shear zone development.

Fluid is focussed down through the fault towards the cover-basement interface (Fig. 6.8a) and beneath, towards dilating areas in the basement, where it meets upward migrating fluids form the basement (Fig. 6.8b). At later stages of deformation (6%) pore pressures decrease further to subhydrostatic levels (particularly in the basement) and flow continues to be focussed down through the more permeable fault (Fig. 6.9a). Failure states within the model show a

preference for tensile failure near the top of the model and elsewhere shear failure with trends similar to the orientation of the fault (Fig. 6.9b).

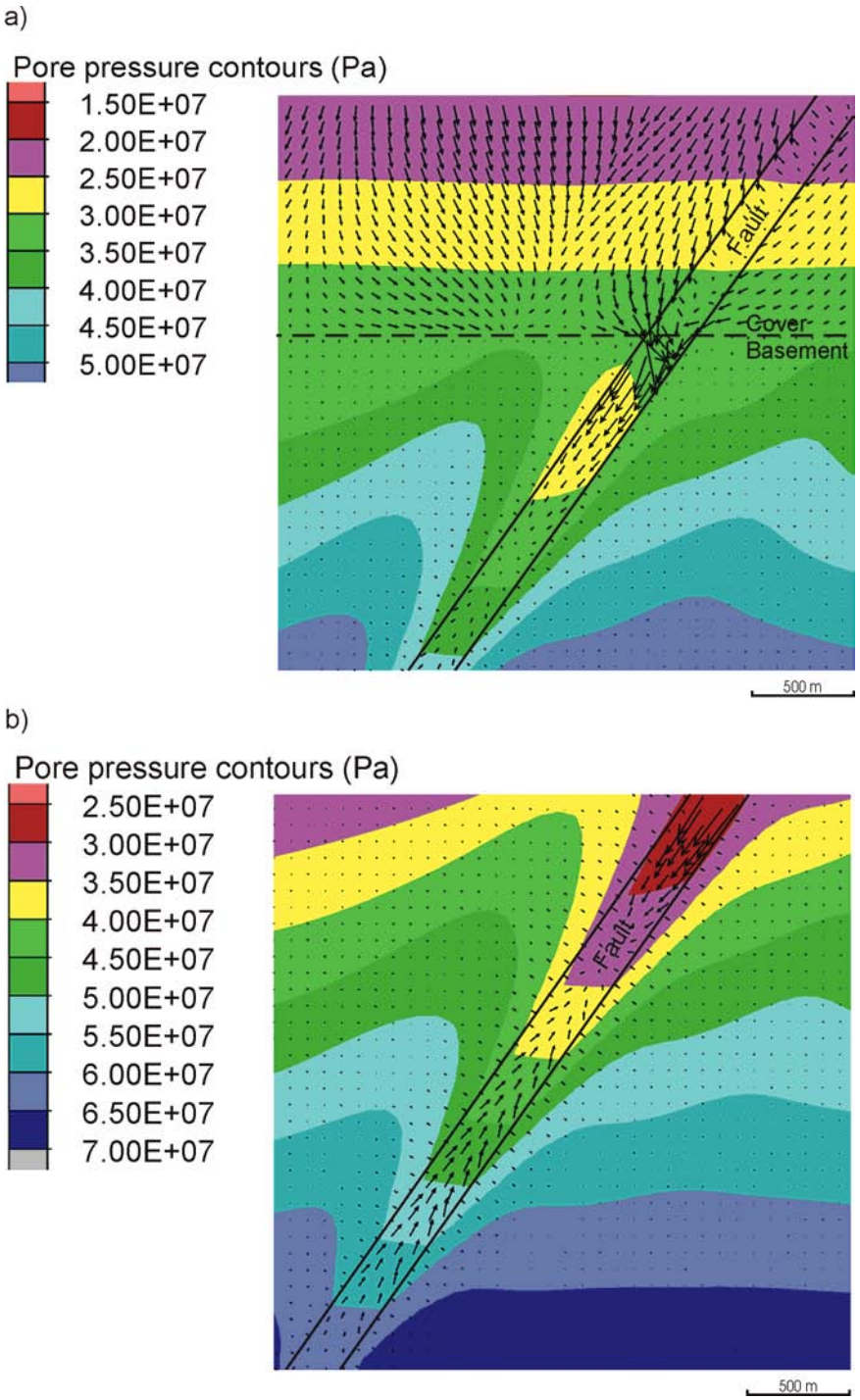

Figure 6.8. Model 2a at 2% extension, **a**) pore pressure contours and fluid flow vectors, displaying a downward migration into the basement, with fluid focussed within the fault and towards areas of low pore pressure, **b**) pore pressure contours and fluid flow vectors, displaying upward flow from the base of the fault which meets downward migrating fluids, primarily driven by pore pressure gradients and dilatancy.

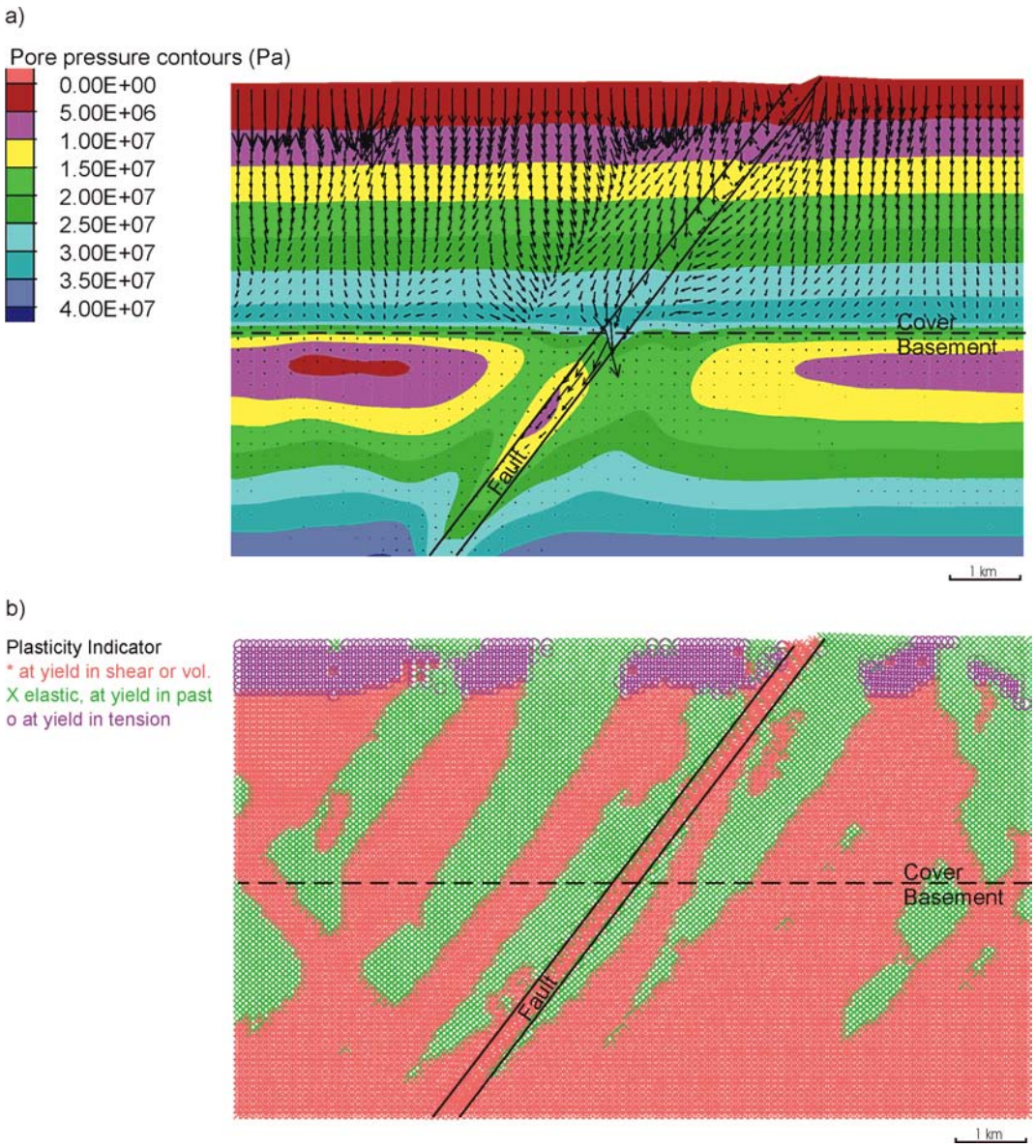

Figure 6.9. Model 2a at 6% extension, **a**) pore pressure contours and fluid flow vectors, displaying a downward migration into the basement and fluid is focussed within the fault. Subhydrostatic pore pressures are evident within the less permeable basement, and in particular lowest areas are found just below the interface, **b**) state of yield for the model at 6% extension, mostly at yield in shear, with tensile failure limited to the top of the model.

6.6.4 Model 2b (Extension - Hydrostatic pore pressure with short fault)

The results of this model are very similar to the previous model (Model 2a), with shear bands developing in similar locations (Fig. 6.10a) and pore pressure decreasing during extension (Fig. 6.10b). Interestingly, pore pressure is slightly higher than that of the previous model (by around 5 to 10 MPa) (Fig. 6.11a)

which may be an artefact of the fault not being in contact with the boundary of the model. Another interesting point is the fact that there is no upward flow through the base of the fault presumably due to very low basement permeability (Fig. 6.11b).

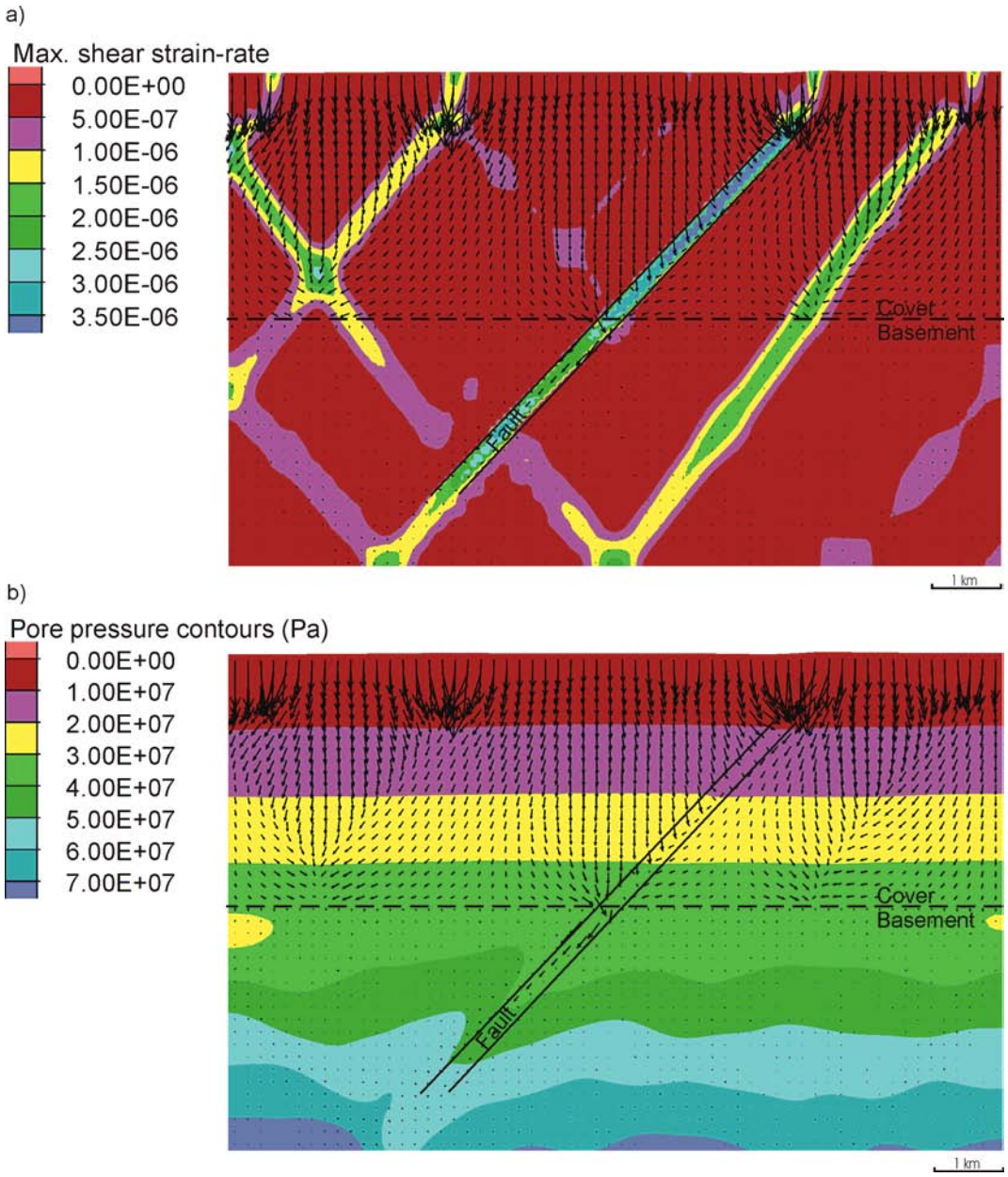

Figure 6.10. Model 2b at 2% extension, **a**) shear strain rate showing maximum values in the fault which coincides with maximum dilation and result in fluid flow focussing. These results are very similar to Model 2a, **b**) pore pressure contours and fluid flow vectors, displaying a decrease in pore pressure in the basement to subhydrostatic pressures, and fluid focussed within the fault in a downward path.

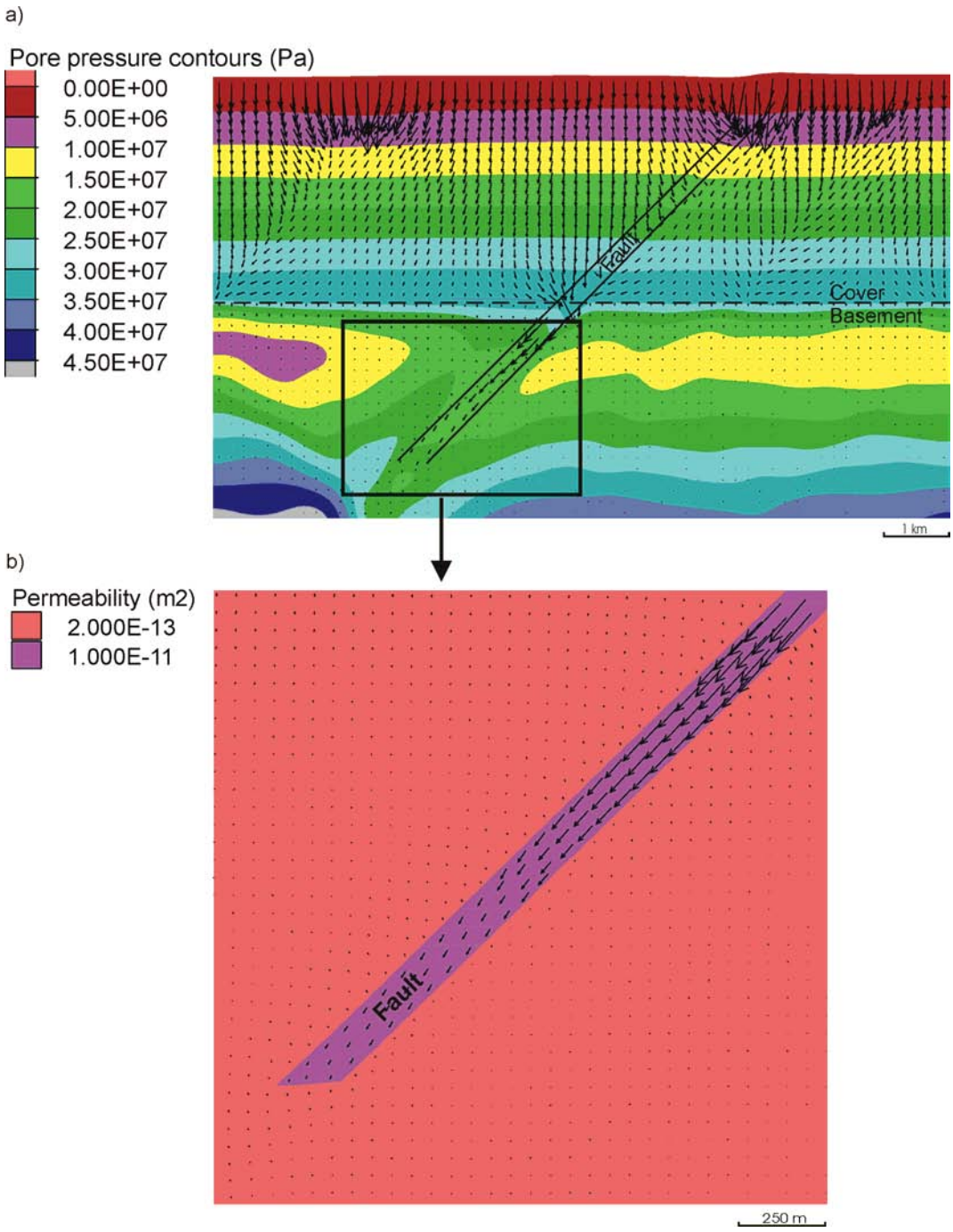

Figure 6.11. Model 2b at 6% extension, **a**) pore pressure contours and fluid flow vectors, displaying a decrease in pore pressure in the basement to subhydrostatic values, and fluid focussed within the fault in a downwards path, **b**) relative permeability values of the geological units and fluid flow vectors, indicating strong flow within the more permeable fault and no fluid entering the fault from the base due to pore pressure gradients and low permeability of the basement.

6.6.5 Model 2c (Extension - Lithostatic pore pressure in the basement with short fault)

The initiation of lithostatic pore pressure in the basement of this model has resulted in a variation in the distribution of strain relative to the previous model (Model 2b) (Fig. 6.12a). Fluid flow is primarily upwards from the basement and through the more permeable fault; however, fluids in the cover are migrating downwards towards the interface (Fig. 6.12b).

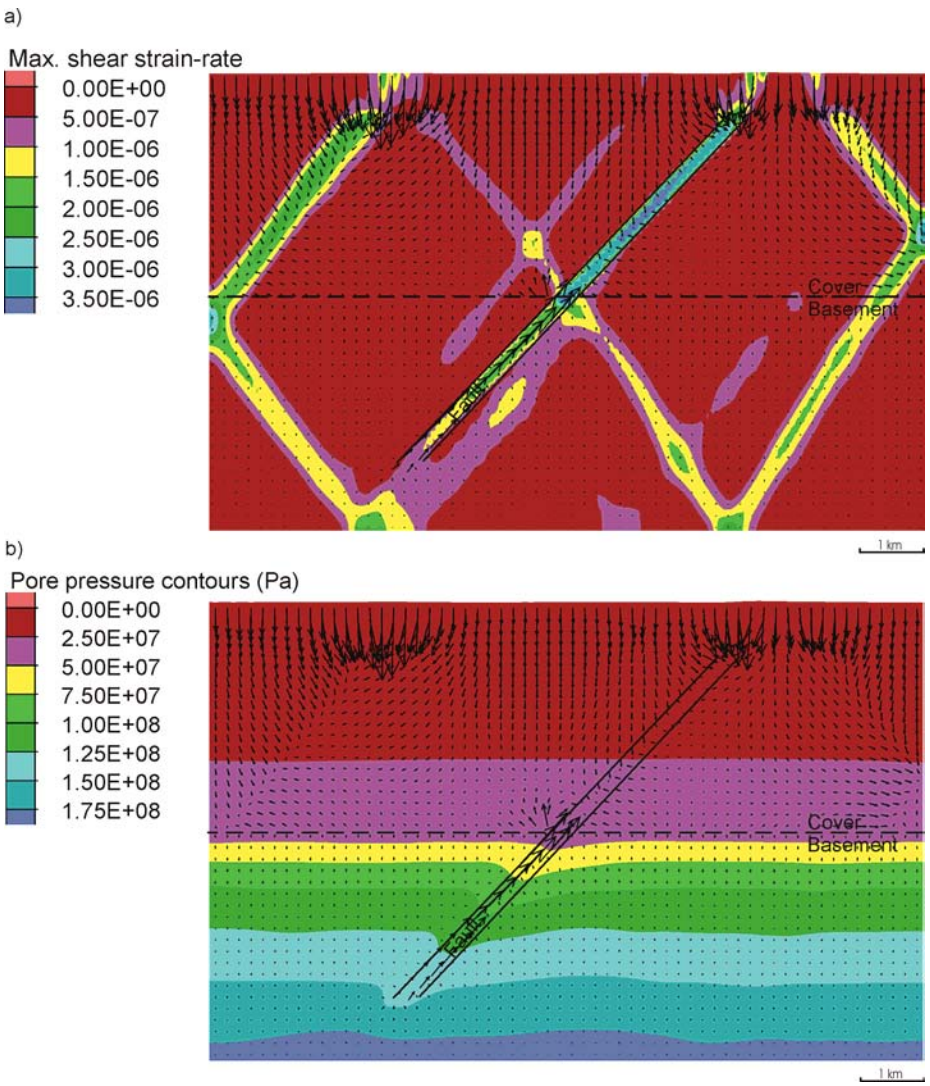

Figure 6.12. Model 2c at 2% extension, **a**) shear strain rate showing maximum values in the fault and displaying a variation in the distribution of shear bands relative to Model 2b, **b**) pore pressure contours and fluid flow vectors, displaying a decrease in pore pressure in the basement and fluid focussed within the fault. Fluid flow is primarily upwards in the basement and mostly downwards in the cover.

Fluid flow is focussed upwards through the fault until it reaches the covering sediments (Fig. 6.13a), where it is focussed towards areas of dilation and high shear strain (Fig. 6.13b).

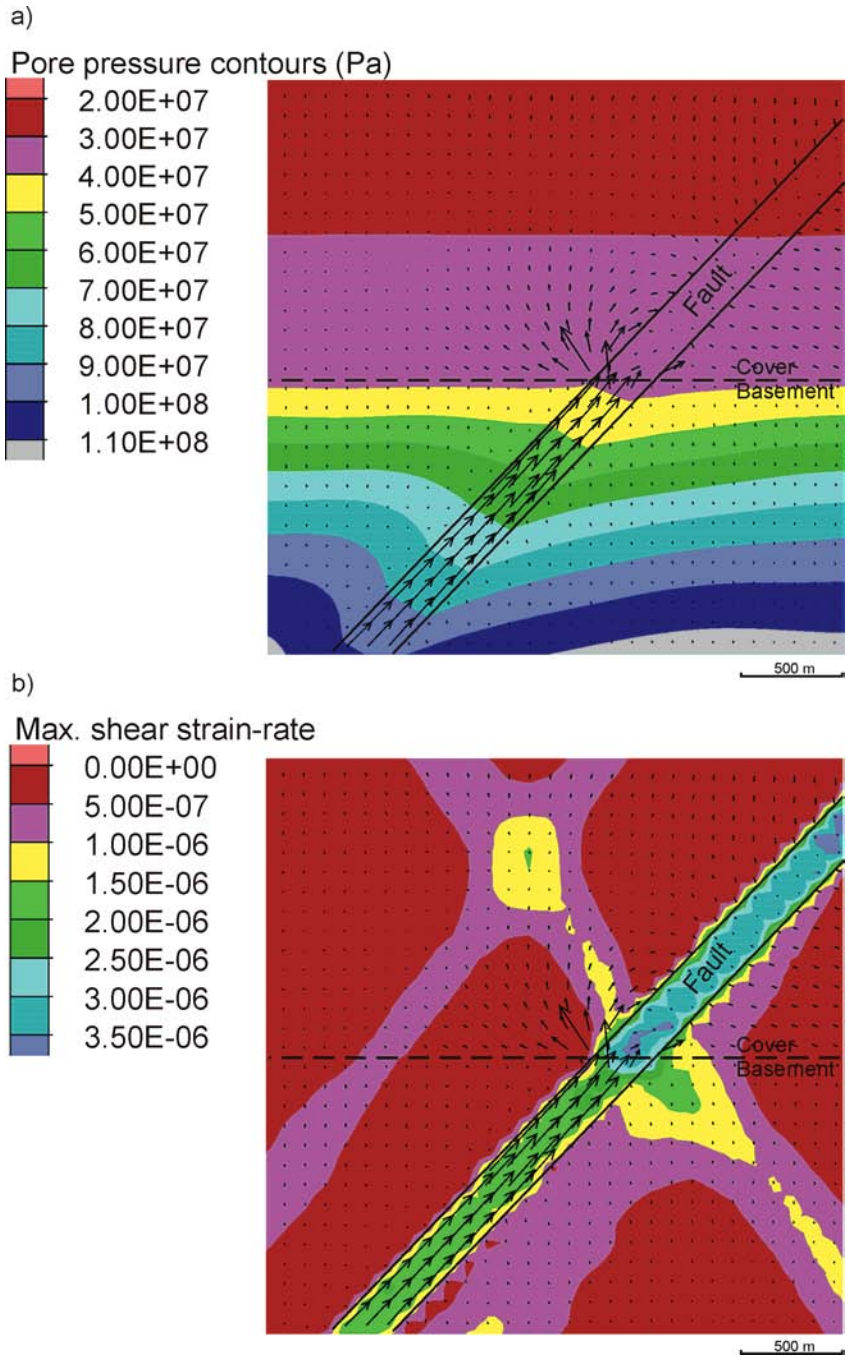

Figure 6.13. Model 2c at 2% extension, **a**) pore pressure contours and fluid flow vectors at the interface and fault, displaying an upward migration into the cover with fluid focussed within the fault until reaching the more permeable cover, **b**) contours of shear strain and fluid flow vectors, displaying upward flow from the basement towards high strain dilating areas.

As extension progresses, we see a continual decay of pore pressure towards hydrostatic values (Fig. 6.14a). As the pore pressures continue to decay we see a change in fluid flow direction from upwards through the basement fault and into the cover (Fig. 6. 14b) to downwards from the cover into the basement (Fig. 6.14c).

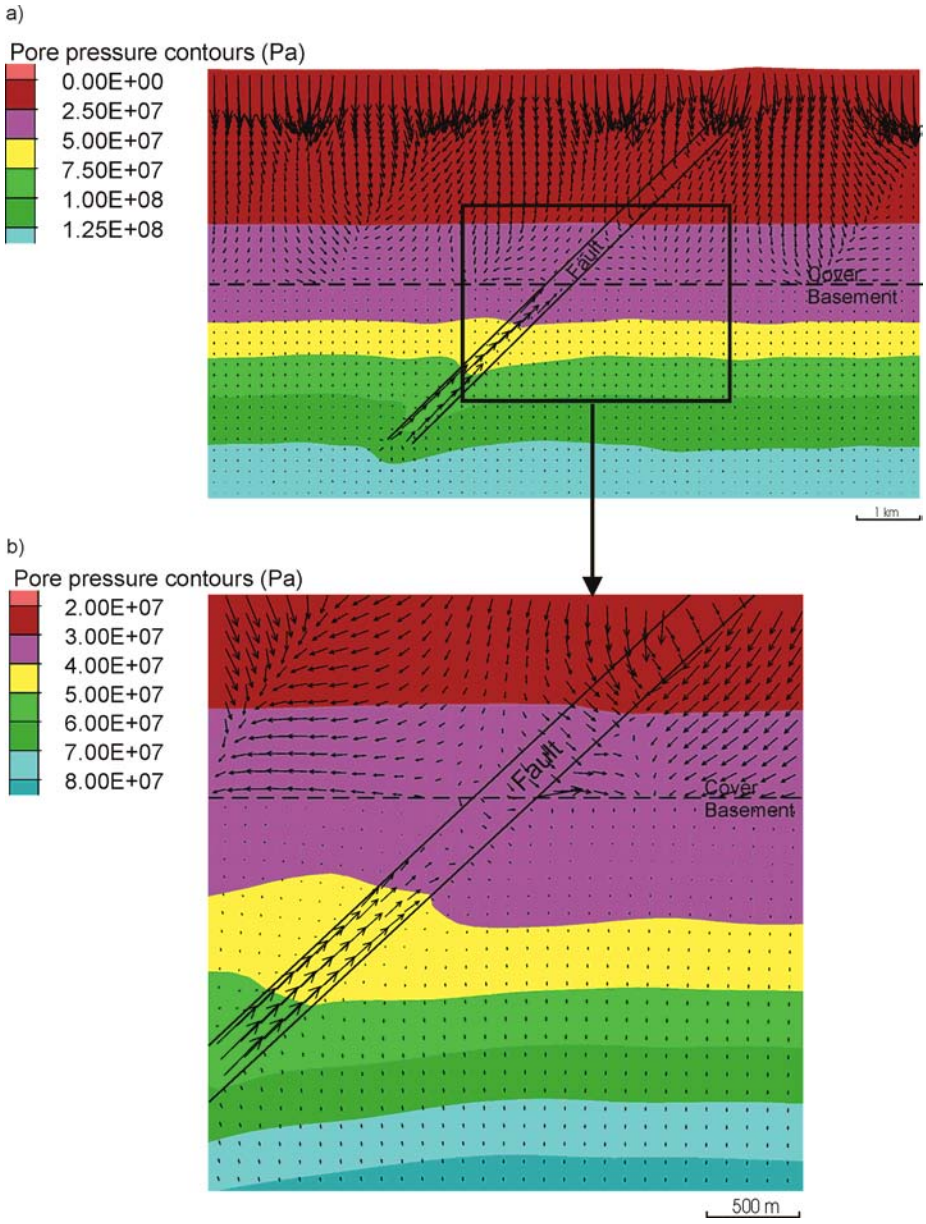

Figure 6.14a,b. Model 2c, **a**) pore pressure contours and fluid flow vectors at 6% extension, displaying an upward migration into the cover with fluid focussed within the fault, **b**) pore pressure contours and fluid flow vectors at 8% extension, displaying an upward migration of fluids within the fault towards the basement-cover interface. Fluid flow within the cover is primarily driven by shear strain and dilatancy.

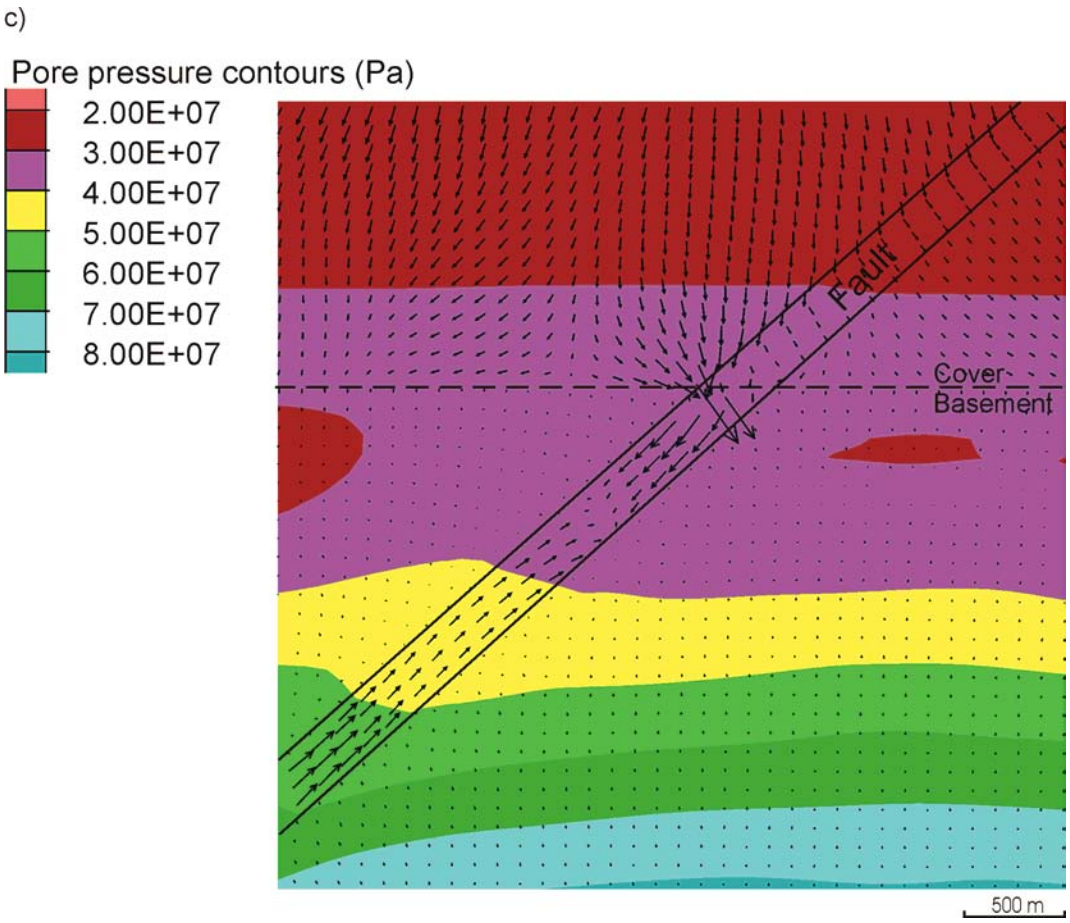

Figure 6.14c. Model 2c displaying pore pressure contours and fluid flow vectors at 10% extension, displaying a downward migration path within the fault and into the basement. Potential fluid mixing zones are evident within the fault.

6.6.6 Model 2d (Extension - Lithostatic pore pressure in the basement with basement only fault)

As a result of restricting the fault to the basement only and applying a lithostatic pore pressure to the basement; we see a significant difference in the distribution of strain relative to previous models (Fig. 6.15a). In contrast to the previous models, areas of highest strain rates are not found in the fault, but adjacent and parallel to the fault. Fluid flow is forced up through the fault due to the pressure gradients in the model, entering the covering sediments and focussing towards areas of high strain (Fig. 6.15b).

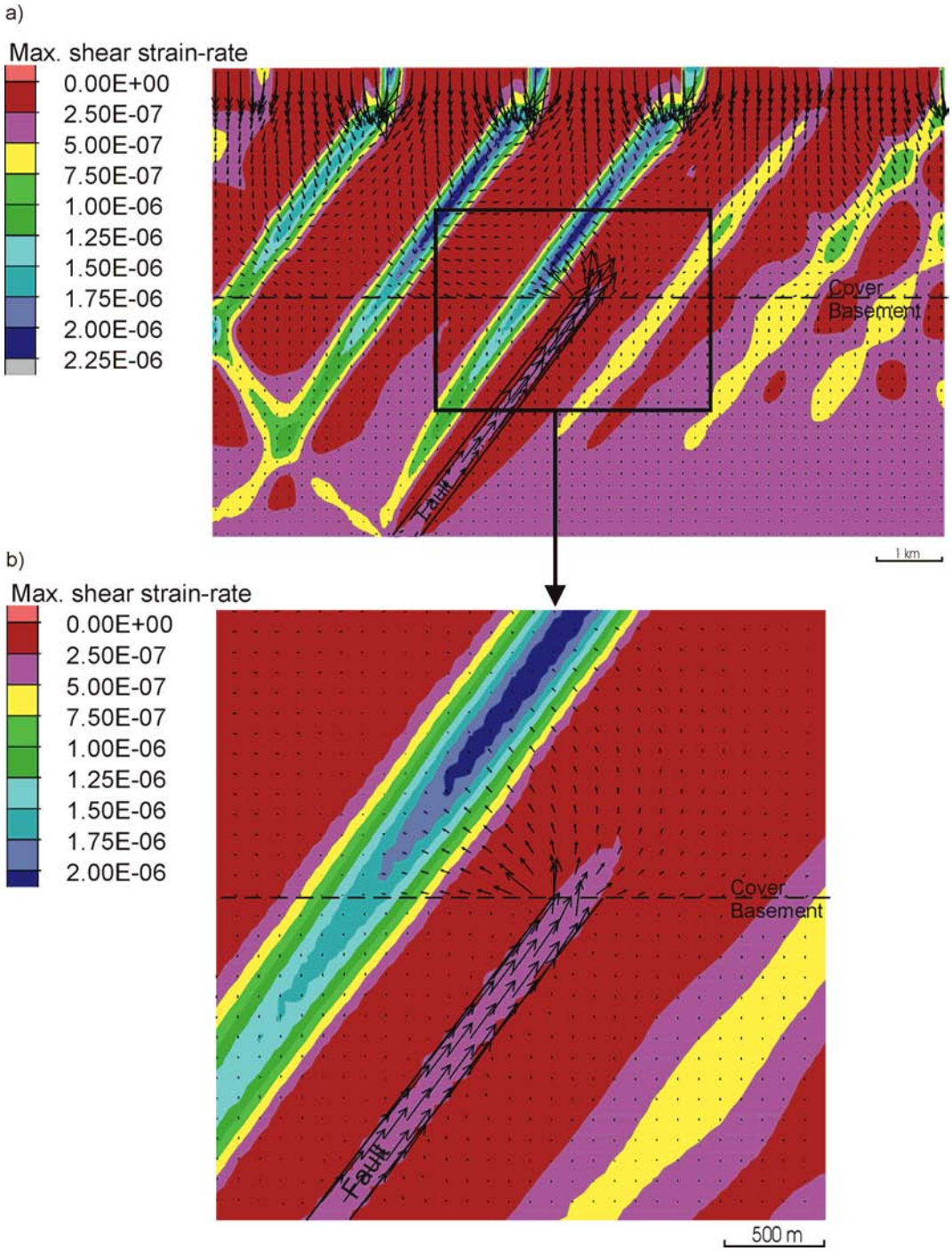

Figure 6.15. Model 2d at 2% extension, **a**) shear strain rate showing maximum values outwith the fault, in contrast to previous models. Shear bands are forming adjacent and parallel to the fault which are focussing fluids, **b**) magnification at the interface displaying shear strain rate showing maximum values outwith the fault. Fluid is focussed within the fault and flow direction is primarily upwards from the basement into the cover and towards high strain zones.

Pore pressure within the model decreases, decaying towards hydrostatic values in the basement, and maintaining the gradient in the cover (Fig. 6.16a). As the fluid flow enters the covering sediments it is directed towards areas of dilation, which correspond with areas of high strain (Fig. 6.16b).

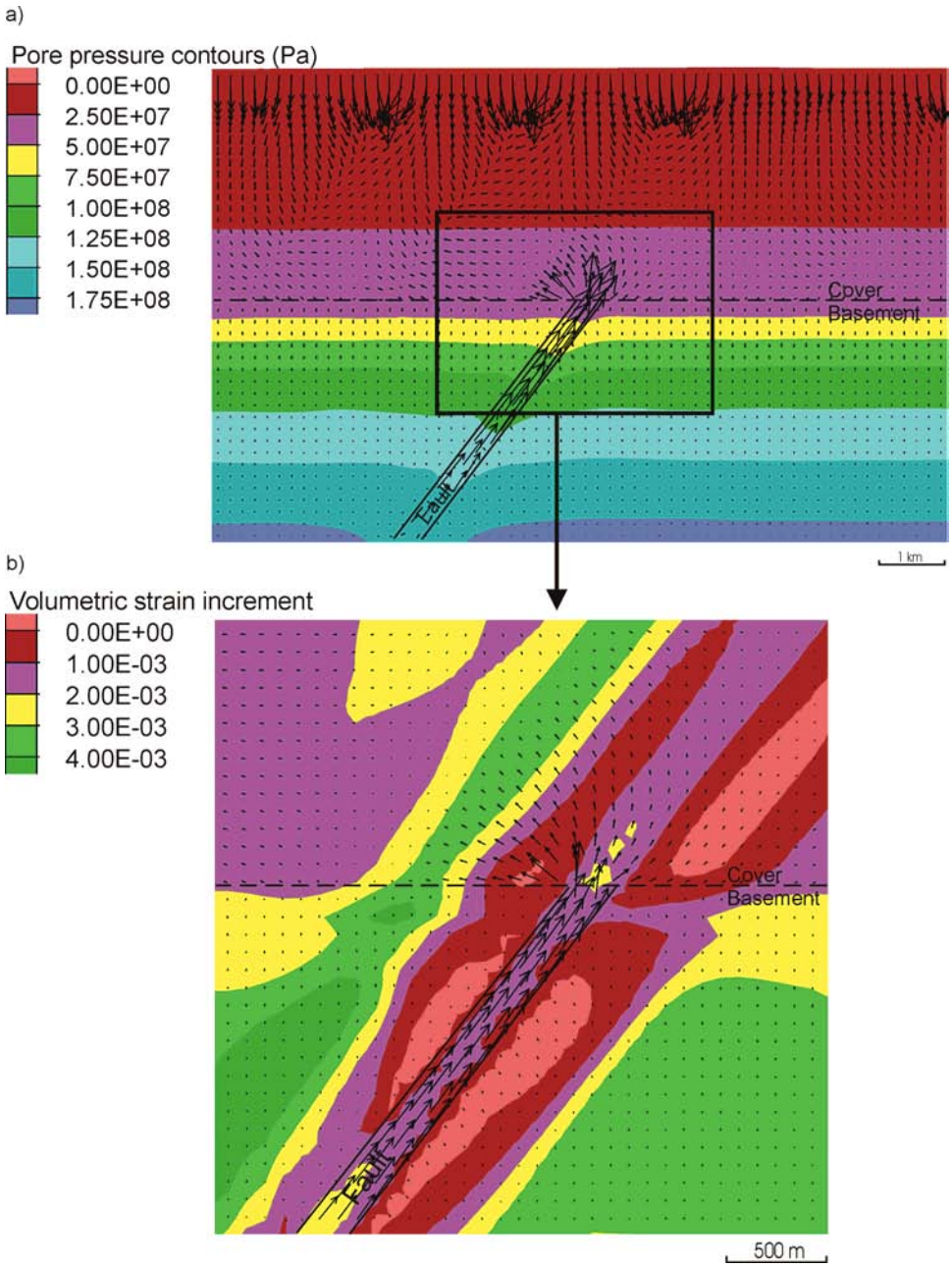

Figure 6.16. Model 2d at 2% extension, **a**) pore pressure contours and fluid flow vectors, displaying an upward migration into the cover with fluid focussed within the fault, pore pressures are decreasing towards hydrostatic values in the basement and maintaining hydrostatic pressure in the cover **b**) volumetric strain (dilation) contours and fluid flow vectors displaying an upward migration into the cover towards dilatant areas.

As deformation continues (10%) we continue to see pore pressures decaying (Fig. 6.17a), particularly in the basement, and this contributes to the shift in upward to downward migrating fluids within the fault (Fig. 6.17b).

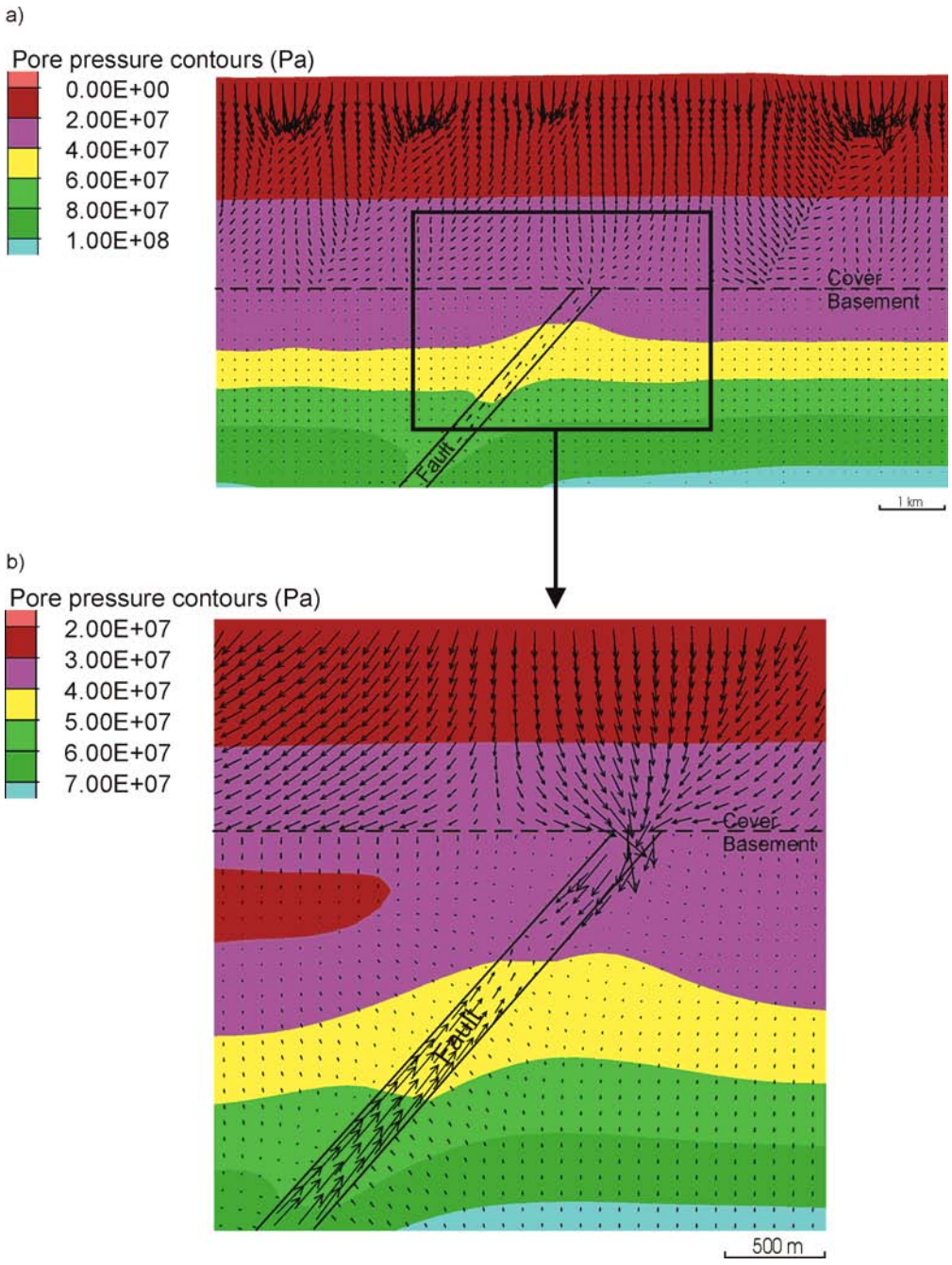

Figure 6.17. Model 2d at 10% extension, **a**) pore pressure contours and fluid flow vectors, displaying an downward migration into the basement, fluid is focussed within shear bands and the fault, pore pressures are decreasing towards hydrostatic values in the basement and maintaining hydrostatic pressure in the cover **b**) pore pressure contours and fluid flow vectors displaying an upward migration from the base of the fault and competing with downward migrating fluids from the cover.

6.6.7 Strain Rate Variations

As a result of the notable decrease in pore pressure in many of the models, strain rates were tested to evaluate the mechanical reasons for such rapid decay, particularly within the basement material, and to determine the most realistic geological scenario for this behaviour. Strain rates for the previous models ranged between 3.34e-10 sec^{-1} to 1.33e-11 sec^{-1}. To decrease the strain rate in comparison with fluid rates we firstly decreased the bulk displacement per step in two models (12 km wide), from 0.0024 m to 0.00024m, to 0.000024 m, and then increased the number of fluid steps to mechanical steps to a ratio of (1 mechanical step to 10 fluid steps), in an attempt to reduce the rapid decay of pore pressure and maintain equilibrium and plastic flow. Unfortunately, the downside of decreasing the strain rate is a significant increase in computational time, with some models requiring weeks to complete. The conclusive findings from the strain rate sensitivity analysis were as a follows:

a) Fast strain rates (~1.0e-9 sec^{-1}) resulted in early increased failure within the Mohr Coulomb material and pore pressure within the models decreased rapidly.
b) Slow strain rates (~1.0e-15) resulted in only limited failure with no shear bands evident, with the model mostly in an elastic state. Pore pressures maintained a hydrostatic equilibrium.
c) Medium strain rates (1.0e-11 to 1.0e-13) led to a combination of failure (shear and tensile) and development of shear bands, causing eventual deformation-induced flow and a slow decay in pore pressure towards

hydrostatic in models with initial lithostatic pressure. For models with initial hydrostatic fluid pressure, eventually subhydrostatic gradients and downflow occurred in basement rocks.

We decided to confirm that the FLAC software was adequately dealing with the hydro-mechanical processes that the models were exhibiting, and if there was an alternative numerical method for dealing with a faster convergence rate and less computational time. To do this we calculated the Biot modulus (M) and stiffness ratio (Rk). If M_f is much larger than M_s or Rk is much greater than 1 then the stable theoretical mechanical time step becomes extremely small in comparison to the time required to reach steady state. Calculations were as follows:

$$M_f = \frac{K_f}{n} \qquad M_s = \frac{K_s}{n}$$
$$= \frac{2e9}{0.3} = 6.66e9 \qquad = \frac{4.95e10}{0.3} = 1.65e11 \tag{6.1}$$

where K_f is the bulk modulus of the fluid, K_s is the bulk modulus of the solid, and n is the porosity of the solid.

$$Rk = \frac{\frac{K_f}{n}}{K_s + \frac{4G}{3}}$$
$$= \frac{6.66e9}{8.91e10} = 0.0747 \tag{6.2}$$

where K_f is the bulk modulus of the fluid, K_s is the bulk modulus of the solid, n is the porosity of the solid, and G is the shear modulus of the solid material. As a result of the calculations, the solid medium is much stiffer than the fluid (i.e. realistic) and therefore there is no obvious way to speed up convergence of the models. It would appear that the algorithm currently used in FLAC for calculating convergence of a hydro-mechanical process, in this instance, is optimal.

6.7 Discussion and Conclusions

Deformation in rocks usually results in a net increase (extension) or decrease (contraction) of volume space at some point during the deformation process, and hence, affects fluid pressures in these areas. We can observe this in a simple contraction scenario, where contraction decreases pore space therefore increases fluid pressure. In extension the opposite response is plausible, such that an increase in volume would result in lowering pore pressure as the fluid attempts to expand and fill the newly created volume. In FLAC, any permeable boundary of the model would be required to draw fluid in to maintain pore pressures in a fully saturated condition; however, in an impermeable rock this may cause problems as fluid cannot migrate as quickly as it would in a more permeable medium. This circumstance might be unrealistic in low strain geological process, where typical '***average***' values for geologically acceptable strain rates range from 1.00e-13 sec^{-1} to 1.00e-17 sec^{-1} (e.g. Pfiffner & Ramsey, 1982; Kuznir & Park, 1987; Lynch & Morgan, 1987; Tadakazu, 2001; Pietrantonio & Riguzzi, 2004). However, laboratory studies have shown strain rates in olivine crystals as high as 1.00e-9 sec^{-1} (Turcotte & Schubbert, 2002),

and in many cases zones of high strain rate might be expected in any heterogenous crust undergoing slow average bulk strains. Hence, these models may be indicating a realistic response to geological processes in deep crustal/mantle environments or in processes such as earthquakes. There is recent evidence in the literature of under-pressured basement material (e.g. Integrated Ocean Drilling Program; Kastner & Malone, 2004; Stober & Bucher, 2004), with subhydrostatic pressures having also been linked to faulting events (Sleep & Blanpied, 1992). Numerical models showing local mechanically induced subhydrostatic pore pressures are also a consequence of contraction of heterogeneous materials, when the bulk pore pressure gradient is much greater than hydrostatic (e.g. Ord & Oliver, 1997). In any instance where there is relatively rapid deformation processes underway, particularly within a low permeability material (e.g. granite basement), it appears mechanically feasible to expect a period during this deformation where the rocks will be under-pressured and may display subhydrostatic pore pressures. However, this would most likely not be sustained for long periods as fluids from surrounding rocks would migrate towards areas of low pressure in an attempt to maintain at least a hydrostatic equilibrium state. The key elements here are the rates of fluid migration through media in comparison to the rates of deformation.

During episodic faulting, as a consequence of extensional deformation, low permeability materials (e.g. basement), may not have the ability to allow localised fluids to migrate quickly enough in response to the deformation, therefore providing subhydrostatic pore pressures that would facilitate downward migrating fluids from shallower depths (e.g. sedimentary basins).

This process may provide a mechanism for the migration of basinal brines to scour basement during episodic deformation. If pore fluid pressures then increased to suprahydrostatic levels (e.g. by granite emplacement), the release of these fluids in upward migrating pulses could facilitate a return of metal rich fluids to the basin above.

The numerical modelling presented here provides insight into the potential mechanical responses of short term (fast strain rates) geological processes such as faulting and potentially earthquake activity. It is apparent that if the rate of these deformation processes is faster than that of the ability for fluid to move through the rock mass (e.g. impermeable basement), then relatively quick decay to subhydrostatic pore pressures and downward migration of fluids is possible. Within the models we see a preference for fluids to focus towards areas undergoing high strain and dilation, which dominates the overall pattern of flow. Topography does have an influence over downward flow, particularly in permeable cover rocks. Very little flow is observed from the basin sediments into the basement for most models, primarily due to the permeability contrasts. This supports the commonly accepted generation of overpressure in the deep basin during compaction, as an effective downward barrier or seal may be formed due to the low permeability of the basement material. However, when permeable structures such as a faults or shear zones are present across the interface, we see a transfer of fluid and pore pressure attempts to equilibrate.

In conclusion, downward migration of fluids is a natural consequence of the extension of dilatant materials where strain rates are high. However, fluid

migration downwards across the interface requires a permeable conduit such as a fault or shear zone. Slower strain rates aid in maintaining pressure gradients, allowing time for the system to equilibrate. However, rapid decreases in pressure as a result of dilation and failure may provide mechanisms for mass transfer across basement-cover interfaces, which may be one explanation for the derivation of base metals with 'basement' isotopic signals in many mineralised basinal settings. Other alternatives relate to thermal structure. Work in progress suggests buoyancy due to fluid viscosity (and density) decreases by heating, and may produce driving forces for fluid flow at approximately the same order of magnitude as deformation induced dilatancy.